

FURTHER OBSERVATIONS OF ROTATIONALLY EXCITED FAR-INFRARED ^{16}OH AND ^{18}OH EMISSION IN ORION-KL: TIGHTER CONSTRAINTS ON THE NATURE OF THE EMITTING REGION

G. J. MELNICK,¹ G. J. STACEY,² R. GENZEL,³ J. B. LUGTEN,² AND A. POGLITSCH³

Received 1989 April 24; accepted 1989 July 1

ABSTRACT

We have observed the region within 1 arcmin of Orion-KL and report the first detections of the ^{16}OH ${}^2\Pi_{1/2} \rightarrow {}^2\Pi_{3/2}$ $J = 3/2^- \rightarrow 3/2^+$ rotational cross-ladder transition (53.351 μm) and the ^{18}OH ${}^2\Pi_{3/2}$ $J = 5/2^+ \rightarrow 3/2^-$ rotational ground-state transition (120.1719 μm). We find that both of these lines exhibit a P-Cygni profile and unambiguously show that the OH gas is expanding out from the central BN/KL infrared cluster. In addition, we have velocity resolved the ^{16}OH ${}^2\Pi_{3/2}$ $J = 5/2^- \rightarrow 3/2^+$ rotational ground-state transition (119.234 μm) and find that its intrinsic full-width at half-maximum (FWHM) is 75 km s^{-1} . We model both the line fluxes and line profiles, along with the previously measured ^{16}OH ${}^2\Pi_{3/2}$ 84 μm and ${}^2\Pi_{1/2}$ 163 μm rotational transitions, and find that no single temperature and density component can reproduce the data. Rather, the best overall fit to the data requires emission from three main components of the gas: (1) postshocked gas with the profiles of temperature, density, and OH abundance like that predicted by Draine and Roberge (1982) for a 38 km s^{-1} C-type shock; (2) a higher density ($n[\text{H}_2] \simeq 2 \times 10^7 \text{ cm}^{-3}$) component to the cool postshocked region than given by Draine and Roberge; and (3) the plateau region. All three components require a significant radiative background in order to fit the data.

Subject headings: infrared spectra — interstellar molecules: nebulae: individual (Orion Nebula)

I. INTRODUCTION

^{16}OH far-infrared line emission from excited rotational states was first detected toward the embedded star-forming region in Orion-KL by Storey *et al.* (1981). Though the OH line widths were unresolved in these early measurements, two observational features led these authors to assume that the OH ${}^2\Pi_{3/2}$ $J = 5/2 \rightarrow 3/2$ 119 μm emission they detected comes from the shocked gas region surrounding BN/KL: (1) the emitting region had to be warm since the OH lines were seen in emission and the temperatures above the ground state for the upper $J = 5/2$ levels are $\simeq 121$ K and, (2) the OH emission was observed 30" north of KL, toward the peak of the shock-excited H_2 emission (e.g., Beckwith *et al.* 1978). Subsequent observations, with improved spectrometer sensitivity and spectral resolution, have resulted in the detection of two additional far-infrared, rotational doublet transitions: the ${}^2\Pi_{3/2}$ $J = 7/2 \rightarrow 5/2$ lines at 84.4202 and 84.5966 μm and the ${}^2\Pi_{1/2}$ $J = 3/2 \rightarrow 1/2$ lines at 163.121 and 163.396 μm (Watson *et al.* 1985; Viscuso *et al.* 1985a; Viscuso *et al.* 1985b; Melnick *et al.* 1987). Unfortunately, even with the detection of six OH far-infrared rotational transitions, it was not possible to distinguish between a variety of different models for the emitting region, including shocks and a number of nonshock scenarios (see Melnick, Genzel, and Lugten 1987, hereafter referred to as Paper I, for a review of these models).

In this paper, we present the first observations of two additional OH far-infrared transitions, the ^{16}OH ${}^2\Pi_{1/2} \rightarrow {}^2\Pi_{3/2}$ $J = 3/2^- \rightarrow 3/2^+$ cross-ladder transition at 53.351 μm (see Fig. 1) and the ^{18}OH ${}^2\Pi_{3/2}$ $J = 5/2^+ \rightarrow 3/2^-$ rotational ground-state transition at 120.1719 μm , plus a spectrum of the previously observed ^{16}OH ${}^2\Pi_{3/2}$ $J = 5/2^- \rightarrow 3/2^+$ 119.234 μm

line which has now been velocity resolved. Because the intensities and profiles of these lines are sensitive to the radiative background, density, temperature, and gas velocity, these transitions can now be used to considerably narrow the range of conditions in the OH emitting region. Here we present a model of the OH emitting regions which successfully accounts for the observed line emission.

II. OBSERVATIONS AND RESULTS

The observations were carried out 1986 November and 1987 January using the 91 cm telescope aboard the Kuiper Airborne Observatory. The data were taken with the Mk II UCB cryogenic tandem Fabry-Perot spectrometer (Lugten 1987). The spectra were obtained with the beam centered on the Becklin-Neugebauer object ($\alpha_{1950} = 5^{\text{h}}32^{\text{m}}46.7^{\text{s}}$, $\delta_{1950} = 5^{\circ}24'17''$). The ^{16}OH ${}^2\Pi_{3/2}$ $J = 5/2^- \rightarrow 3/2^+$ 119.234 μm spectra were taken at resolutions (FWHM) of 40 and 24 km s^{-1} , while the ^{16}OH ${}^2\Pi_{1/2} \rightarrow {}^2\Pi_{3/2}$ $J = 3/2^- \rightarrow 3/2^+$ transition at 53.351 μm and the ^{18}OH ${}^2\Pi_{3/2}$ $J = 5/2^+ \rightarrow 3/2^-$ line at 120.1719 μm were observed with spectral resolutions of 38 and 55 km s^{-1} , respectively. Because of terrestrial O_3 and H_2O absorption, neither the accompanying ^{16}OH ${}^2\Pi_{1/2} \rightarrow {}^2\Pi_{3/2}$ $J = 3/2^+ \rightarrow 3/2^-$ 53.261 μm nor ^{18}OH $J = 5/2^- \rightarrow 3/2^+$ 119.9659 μm transitions was observed.

The telescope's secondary was chopped at a frequency of 33 Hz with an amplitude of 3/7 in azimuth (approximately east-west). The line fluxes were derived from the measured line-to-continuum ratio and the photometric measurements of Orion-KL (M. Werner, private communication). Table 1 summarizes our results along with selected previous observations of OH from Orion-KL (a more complete listing of previous OH rotational data is provided in Paper I). The spectra of the individual OH lines are shown in Figures 2–4. The uncertainty in the absolute value of the continuum is the largest source of error and limits the accuracy of the derived fluxes to $\sim 30\%$. The absolute velocity (and wavelength) scale was determined rela-

¹ Harvard-Smithsonian Center for Astrophysics, Cambridge.

² Department of Physics, University of California, Berkeley.

³ Max-Planck Institut für Physik und Astrophysik, Institut für extra-terrestrische Physik, Garching, F.R. Germany.

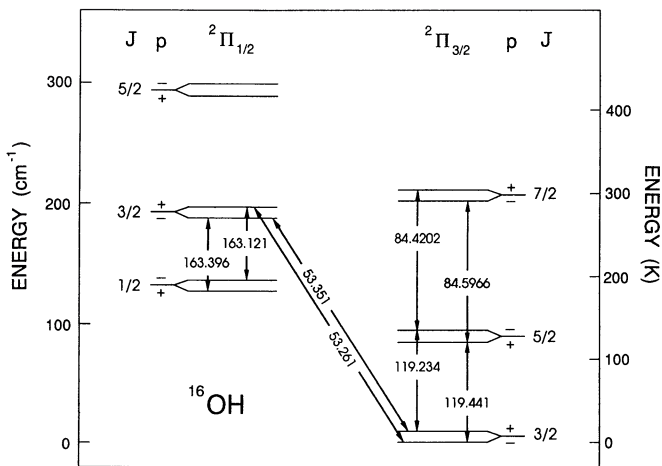


FIG. 1.—Part of the rotational energy level diagram of OH. The rotational ladder has two branches, ${}^2\Pi_{3/2}$ and ${}^2\Pi_{1/2}$, because of spin splitting. The Λ -doubling, which splits each rotational level into two sublevels, is not drawn to scale (the hyperfine splitting that gives rise to the maser transitions is not shown). Both the level J -value (J) and parity (p) are also indicated. The transitions of interest here are marked with solid lines along with the wavelength in microns.

tive to H_2S ($53.3242 \mu\text{m}$), HD^{18}O ($119.3950 \mu\text{m}$), and D_2O ($120.2554 \mu\text{m}$) absorption in a gas cell and is accurate to $\pm 3 \text{ km s}^{-1}$.

The three main results of our most recent observations are:

1. We report the first detection of an OH cross-ladder transition. The ${}^{16}\text{OH}$ $53.351 \mu\text{m}$ line is observed strongly in absorption in the velocity range between -100 and $+10 \text{ km s}^{-1}$ and more weakly in emission between $+10$ and $+80 \text{ km s}^{-1}$.
2. We have detected the ${}^{18}\text{OH}$ $120.1719 \mu\text{m}$ line, counterpart of the ${}^{16}\text{OH}$ $119.441 \mu\text{m}$ transition. The ${}^{18}\text{OH}$ $120.1719 \mu\text{m}$ line is observed in absorption in the velocity range between approximately -100 and $+10 \text{ km s}^{-1}$ and possibly in emission between about $+10$ and $+80 \text{ km s}^{-1}$.
3. The previously observed ${}^{16}\text{OH}$ $119.234 \mu\text{m}$ transition was

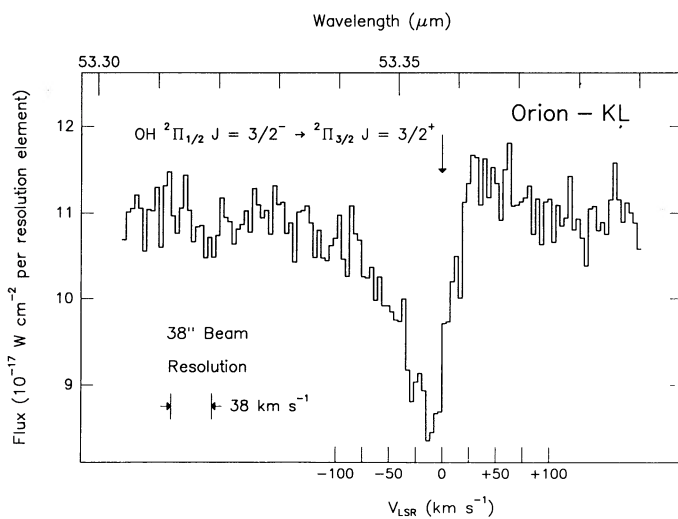


FIG. 2.—Spectrum of the $53.351 \mu\text{m}$ ${}^{16}\text{OH}$ ${}^2\Pi_{1/2} J = 3/2^- \rightarrow {}^2\Pi_{3/2} J = 3/2^+$ cross-ladder transition. The accompanying cross-ladder doublet transition at $53.261 \mu\text{m}$ was not observed because of interference from a terrestrial H_2O absorption feature at $53.2605 \mu\text{m}$.

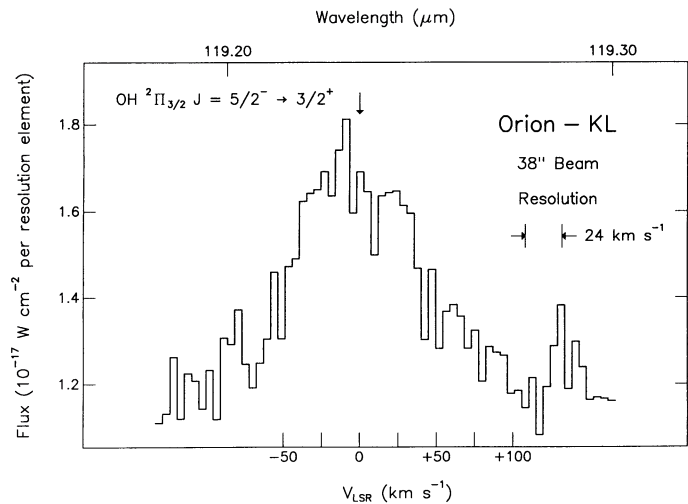


FIG. 3.—Spectrum of the $119.234 \mu\text{m}$ ${}^{16}\text{OH}$ ${}^2\Pi_{3/2} J = 5/2^- \rightarrow 3/2^+$ transition.

reobserved with sufficient spectral resolution, 24 and 40 km s^{-1} , to determine that its FWHM is 75 km s^{-1} . This compares with a FWHM for the $163.121 \mu\text{m}$ line of $\approx 45 \text{ km s}^{-1}$ (Crawford *et al.* 1986). The peak of the $119.234 \mu\text{m}$ line emission occurs at a v_{LSR} of $+10 \text{ km s}^{-1}$.

A number of general conclusions emerge from the data, independent of the model adopted:

1. Assuming that the ${}^{18}\text{OH}$ $120 \mu\text{m}$ transition is optically thin and that the ${}^{16}\text{OH} : {}^{18}\text{OH}$ fractional abundance ratio is $500:1$ (see Comben *et al.* 1986), then, by supposing that all of the ${}^{18}\text{OH}$ is in the upper $J = 5/2^+$ level, the *minimum* ${}^{16}\text{OH}$ column density responsible for the far-infrared emission we detect is determined to be $4 \times 10^{14} \text{ cm}^{-2}$.
2. The relative strengths of the ${}^{16}\text{OH}$ $53.351 \mu\text{m}$ absorption feature and the $163.396 \mu\text{m}$ emission line previously detected (e.g., Melnick *et al.* 1987) clearly demonstrate the importance of radiative excitations. In fact, a comparison of the excitation rate to the ${}^2\Pi_{1/2} J = 3/2^-$ level which is due to the absorption

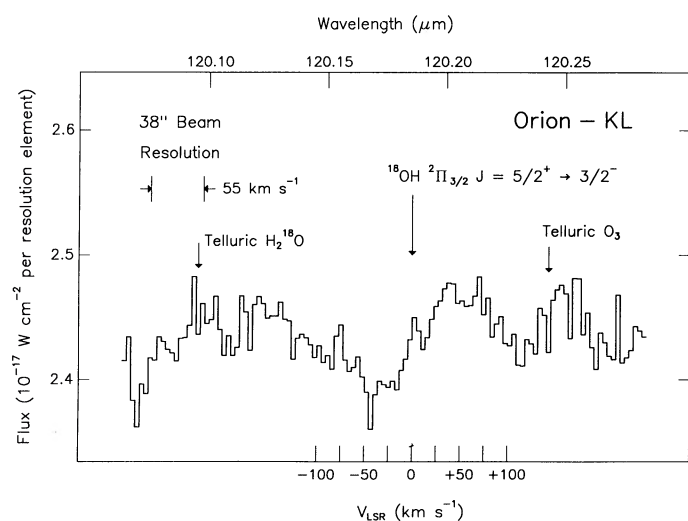


FIG. 4.—Spectrum of the $120.1719 \mu\text{m}$ ${}^{18}\text{OH}$ ${}^2\Pi_{3/2} J = 5/2^+ \rightarrow 3/2^-$ rotational ground-state transition. The accompanying ${}^{18}\text{OH}$ doublet transition at $119.9659 \mu\text{m}$ was not observed because of interference from a nearby terrestrial O_3 absorption feature at $119.9947 \mu\text{m}$.

TABLE 1
SUMMARY OF OH ROTATIONAL DATA USED TO MODEL EMITTING REGION IN ORION-KL

Line	λ (μm)	FWHM Beam Size	Flux in Emission ^{a b}	Flux in Absorption ^{a b}	Intensity in Emission ^{a c d}	Intensity in Absorption ^{a c d}
¹⁶ OH						
² $\Pi_{3/2} J = 7/2^- \rightarrow 5/2^+$	84.5966	1'	1.4 ± 0.4^e	...	1.4	...
² $\Pi_{1/2} J = 3/2^+ \rightarrow 1/2^-$	163.121	55"	$1.3^f g$...	1.6	...
² $\Pi_{3/2} J = 5/2^- \rightarrow 3/2^+$	119.234	45"	$1.88^{h i}$...	3.3	...
² $\Pi_{1/2} J = 3/2^- \rightarrow 2\Pi_{3/2} J = 3/2^+$	53.3512	40"	$0.63^{h j}$	$3.0^{h j}$	1.4	6.6
¹⁸ OH						
² $\Pi_{3/2} J = 5/2^+ \rightarrow 3/2^-$	120.1719	45"	$0.03^{h k}$	$0.06^{h k}$	0.05	0.11

^a Uncertainty in the absolute fluxes and intensities is $\pm 30\%$ unless indicated otherwise.

^b ($10^{-17} \text{ W cm}^{-2}$)

^c Solid angles for different beam sizes are $8 \times 10^{-8} \text{ sr}$ for 55" beam, $5.7 \times 10^{-8} \text{ sr}$ for 45", and $4.5 \times 10^{-8} \text{ sr}$ for 40".

^d ($10^{-3} \text{ ergs s}^{-1} \text{ cm sr}^{-1}$)

^e Viscuso *et al.* 1985a.

^f Melnick, Genzel, and Lugten 1987.

^g Velocity resolution = 60 km s^{-1} .

^h This work.

ⁱ Velocity resolution = 24 km s^{-1} .

^j Velocity resolution = 38 km s^{-1} .

^k Velocity resolution = 55 km s^{-1} .

of 53.351 μm photons, $8 \times 10^3 \text{ photons cm}^{-2} \text{ s}^{-1}$ ($\Leftrightarrow 3 \times 10^{-10} \text{ ergs cm}^{-1} \text{ s}^{-1}$), with the de-excitation rate out of that level via 163.396 μm photons, $1 \times 10^4 \text{ photons cm}^{-2} \text{ s}^{-1}$ ($\Leftrightarrow 1.3 \times 10^{-10} \text{ ergs cm}^{-1} \text{ s}^{-1}$), shows that radiation dominates collisions in exciting the ² $\Pi_{1/2} J = 3/2$ levels.

3. As noted in Melnick *et al.* (1987), the comparable strengths of the 84 and 119 μm lines require that a significant portion of the OH emitting region has temperatures greater than 50 K, densities greater than 10^7 cm^{-3} , or both.

4. The fact that the blueshifted gas is in absorption against the far-infrared continuum in both the ¹⁶OH 53 μm and ¹⁸OH 120 μm spectra unambiguously shows that the OH molecules are in an outflow from the central infrared cluster.

III. CALCULATIONS

In order to model the ¹⁶OH line intensities, the equations of statistical equilibrium and line formation for the lowest 30 levels of the OH molecule have been solved; these include all levels up to the $J = 17/2$ level in the ² $\Pi_{3/2}$ ladder and the $J = 13/2$ level in the ² $\Pi_{1/2}$ ladder. These calculations take account of the Λ -doubling, but ignore the hyperfine structure. The radiative transition probabilities were provided by J. H. Black and E. F. van Dishoeck (1985, private communication) based on the transition matrix elements computed by van Dishoeck (1984). Dewangan, Flower, and Alexander (1987) have calculated the OH-H₂ excitation rate coefficients for the lowest 18 rotational transitions. Downward transition rates are obtained using the principle of detailed balance. Additional rate coefficients were obtained from H. W. Lülf (1985, private communication), Schinke and Andresen (1984), and E. F. van Dishoeck (1985, private communication). In all cases, the downward rate coefficients are taken to be independent of temperature. For lack of any published rate coefficients for ¹⁸OH, the rate coefficients for ¹⁶OH were assumed to apply.

As discussed in § II, radiative processes must be considered along with collisional processes. For Orion-KL, the intensity of the local radiation field is represented by an infrared contin-

uum of the form

$$I_v^c = B_v(T_c) \left[\tau_0 \times \left(\frac{60}{\lambda(\mu\text{m})} \right) \right] \quad (1)$$

where B_v = Planck function at the color temperature of the continuum, T_c . Taking an average value for T_c of 72 K and $\tau_0 = 0.503$ reproduces the 20–100 μm flux density of Orion-KL measured with a 50" beam by Erickson *et al.* (1981) and is consistent with the 400 μm flux density measured with 35 and 90" beam sizes by Keene *et al.* (1982). However, in order to more accurately represent the true distribution of continuum intensity, the analysis that follows assumes that the value of T_c , and thus the continuum strength, increases toward the infrared cluster (e.g., Wynn-Williams *et al.* 1984).

A twofold approach was taken to modeling the OH emitting gas: (1) an attempt was made to fit the data with one gas component, characterized by a single temperature, density, OH abundance, velocity gradient, and radiation background, and (2) a sum was made of the contributions from several known components, such as the shocked gas, plateau, compact ridge, and hot core regions. Conditions characterizing the plateau, compact ridge, and hot core regions have been determined through studies of a variety of molecules and are summarized by a number of authors (e.g., Wynn-Williams *et al.* 1984; Masson *et al.* 1984; Blake *et al.* 1987). Less is known of the conditions that prevail in the shocked gas region where the observed outflowing gas impacts the surrounding quiescent material. In general, the models which come closest to reproducing the existing high- J CO, fine-structure [O I], and rovibrational H₂ lines invoke the presence of a magnetohydrodynamic "C-type" shock (see Draine and Roberge 1982; Chernoff, Hollenbach, and McKee 1982). Though more recent CO and H₂ data have highlighted shortcomings in these C-type models, we use the profiles of temperature, density, velocity, and OH abundance given by Draine and Roberge (1982) as the basis for our shock calculations. Discrepancies between this assumed shock model and the OH data will be discussed in § V.

TABLE 2
BEST-FIT MODEL OF OH EMISSION IN ORION-KL

Component	v_{LSR} (km s^{-1})	Δv (km s^{-1})	T_{gas} (K)	T_c (K)	n_{H_2} (cm^{-3})	OH/ H_2	Diameter ^a (arcsec)	N_{H_2} (cm^{-2})
Plateau	7	30	95	130	2×10^6	2×10^{-7}	20	3×10^{23}
Shock ^b	7	38	2700–30	80	4×10^5 – 7×10^6	2×10^{-5} – 4×10^{-7}	43	3×10^{21} ^c
High-density postshock ^d	7	6	75	80	2×10^7	4×10^{-7}	43	2×10^{22} ^c

^a Assumes that the OH emission fills the area within each component.

^b Calculation of the OH emission from the shocked gas region is based on the profiles of temperature, density, and abundance given by Draine and Roberge 1982.

^c Normal to a single shock surface; assumes that all of the hydrogen is in the form of H_2 .

^d See text.

The geometry of each component is idealized as filled spheres, except for the shocked gas region which was assumed to be a thin, spherical shell. In all cases the gas is assumed to be symmetrically distributed around the central continuum source, i.e., it is assumed that each element of gas see 2π steradians of continuum emission with 50% of the gas in front of the continuum source and 50% of the gas behind the continuum source. Because the measured velocity widths of the OH lines are $> 40 \text{ km s}^{-1}$ (Crawford *et al.* 1986; this work), the radiative transfer in the lines was solved simultaneously with the level populations under the large velocity gradient approximation (Sobolev 1960). In addition to the line intensities, the intrinsic line profiles were calculated from each component. In order to relate these profiles to those observed, the intrinsic line profiles were convolved with a Lorentzian profile with a FWHM equal to the instrumental spectral resolution achieved for each line.

IV. RESULTS OF MODELING

In Paper I, fits to the then available 84, 119, and 163 μm line data were obtained with a number of different single-component models. A reexamination of these models in light of the most recent data indicates that all fail to reproduce the strong 53 μm absorption observed; at the densities suggested for most of those models, i.e., $n_{\text{H}_2} > 5 \times 10^7 \text{ cm}^{-3}$, the profile of the 53 μm line would be mostly in emission and only weakly in absorption. Even our best single-component fit ($T_c = 150 \text{ K}$, $T_{\text{gas}} = 80 \text{ K}$, $n_{\text{H}_2} = 4 \times 10^6 \text{ cm}^{-3}$, and $dv/dr = 500 \text{ km s}^{-1} \text{ pc}^{-1}$) results in a 53 μm profile which exhibits almost equal emission and absorption, contrary to what is observed. Attempts to fit the 53 μm line profile by lowering the gas temperature has the effect of reducing the expected 84 μm line flux below its detected value. We therefore conclude that no single temperature, density, and velocity gradient model adequately reproduces the measured line fluxes and profiles.

Instead, the best fit to the data is obtained by assuming emission from three main regions: (1) the C-type shocked gas region, (2) a dense ($n_{\text{H}_2} \approx 2 \times 10^7 \text{ cm}^{-3}$), warm ($T \approx 75 \text{ K}$) addition to the postshocked region, and (3) the high-velocity plateau. The two postshocked components are assumed to be thin (few $\times 10^{15} \text{ cm}$) concentric shells that, together, have a diameter of $\sim 43''$ —corresponding roughly to the observed separation in both the [O I] 63 μm and $\text{H}_2 v = 1 \rightarrow 0 S(1) 2.12 \mu\text{m}$ emission peaks (Werner *et al.* 1984; Beckwith *et al.* 1978). Moreover, both shocked components are assumed to be subject to an infrared continuum with $T_c \approx 80 \text{ K}$ (see eq. [1]). The high velocity plateau is assumed to be the outflow itself which encompasses the $\Delta v \geq 30 \text{ km s}^{-1}$ gas observed within

about $20''$ of IRC2. Gas this close to IRC2 is assumed to be subject to an average T_c of 130 K (see Werner *et al.* 1977; Genzel and Downes 1982; Goldsmith *et al.* 1983). A summary of these best-fit conditions is given in Table 2.

A comparison of the observed line fluxes and those predicted by this model is shown in Figure 5. The computed line profiles for each contributing component along with the resulting combined profile are shown in Figures 6–9. As is clear from these figures, most of the OH emission we observe arises in the shocked gas region. While agreement with the measured line fluxes could be obtained with only the shocked gas region simply by assuming a somewhat larger shock diameter, the

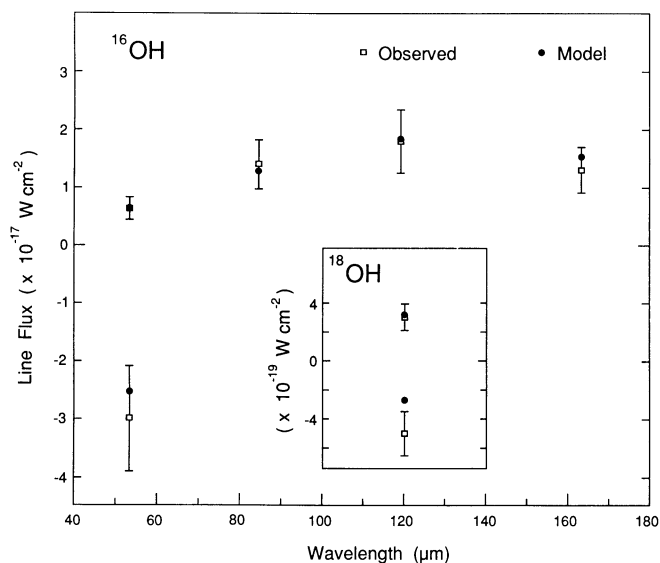


FIG. 5.—Comparison of model OH line fluxes with that observed. The model assumes OH far-infrared rotational line emission from three sources within the Orion-KL region: (1) a $43''$ diameter, 38 km s^{-1} C-type shock like that described by Draine and Roberge (1982) and Chernoff *et al.* (1982), (2) a high density ($n_{\text{H}_2} \approx 2 \times 10^7 \text{ cm}^{-3}$), warm ($T_{\text{gas}} \approx 75 \text{ K}$) zone within the postshock flow and, (3) the $20''$ diameter plateau region. The plateau region is assumed to be subject to an infrared continuum background with $T_c = 130 \text{ K}$, while the shock plus high-density shell which are further from IRC2 are assumed to see a central infrared continuum with $T_c = 80 \text{ K}$ (see eq. [1]). A more complete listing of the best-fit conditions is given in Table 2. The observed OH line fluxes are indicated by the open boxes and the error bars reflect the $\pm 30\%$ uncertainty in each value. The fluxes predicted by the model are shown as dark circles. The ^{16}OH 53 μm and ^{18}OH 120 μm lines, both of which exhibit a P-Cygni profile, are represented by two points each: one for the absorption line flux and the second for the emission line flux.

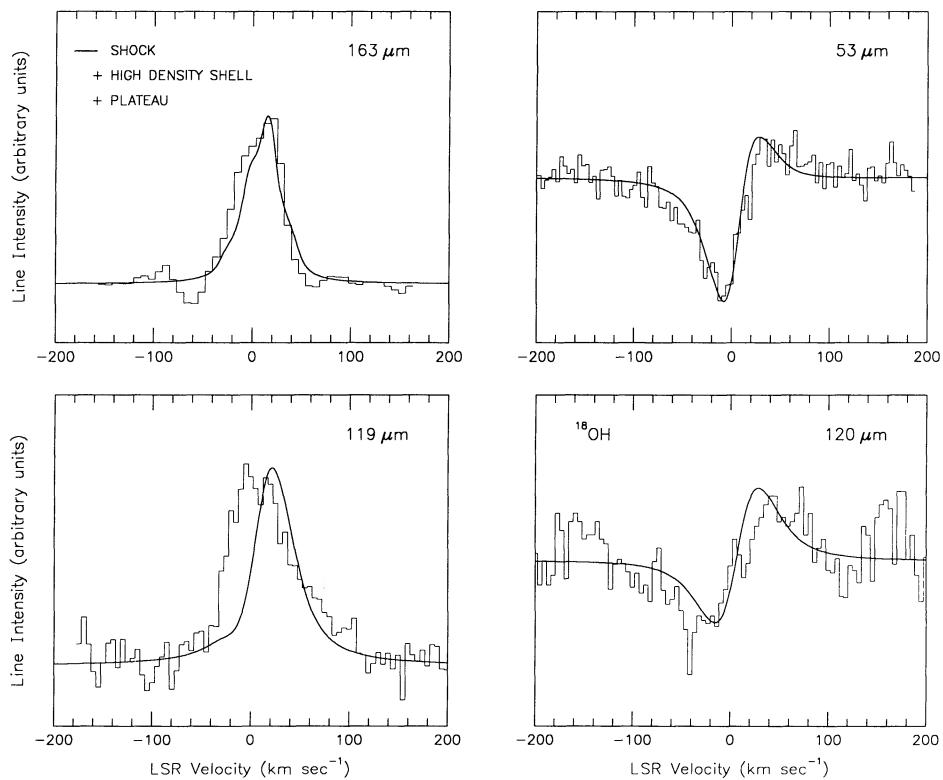


FIG. 6.—OH line profiles resulting from best-fit three-component model described in the text. In order to match the observed profiles, the predicted profiles were convolved with a Lorentzian line shape that has a full-width at half-maximum equal to the instrumental spectral resolution obtained for each line: 38 km s^{-1} at $53 \mu\text{m}$, 40 km s^{-1} at $119 \mu\text{m}$, 15 km s^{-1} at $163 \mu\text{m}$, and 55 km s^{-1} for the ^{18}OH line at $120 \mu\text{m}$. The $163 \mu\text{m}$ observations were obtained previously (Crawford *et al.* 1986). The peaks of the predicted line profiles have been normalized to the data.

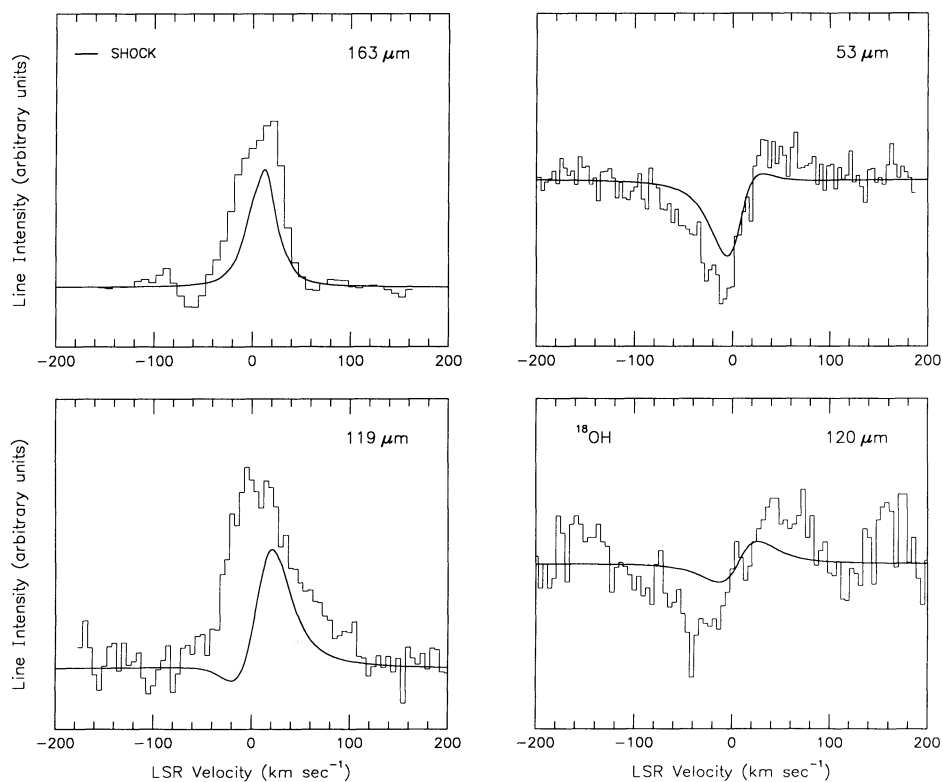


FIG. 7.—Same as Fig. 6, except for the contribution from the C-type shock alone. The intensity scale is the same as that used in Fig. 6, thus permitting a direct assessment of the relative contribution from the shocked gas region to the final line profile.

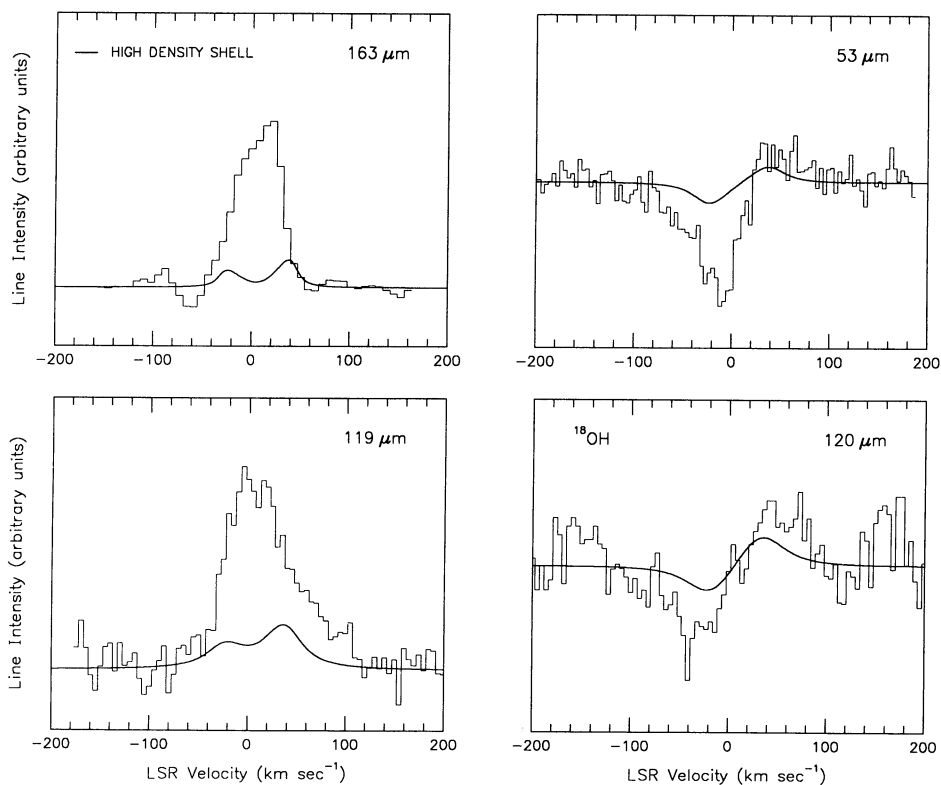


FIG. 8.—Same as Fig. 6, except for the contribution from the high-density postshock gas alone. The intensity scale is the same as that used in Fig. 6, thus permitting a direct assessment of the relative contribution from the high density shell to the final line profile.

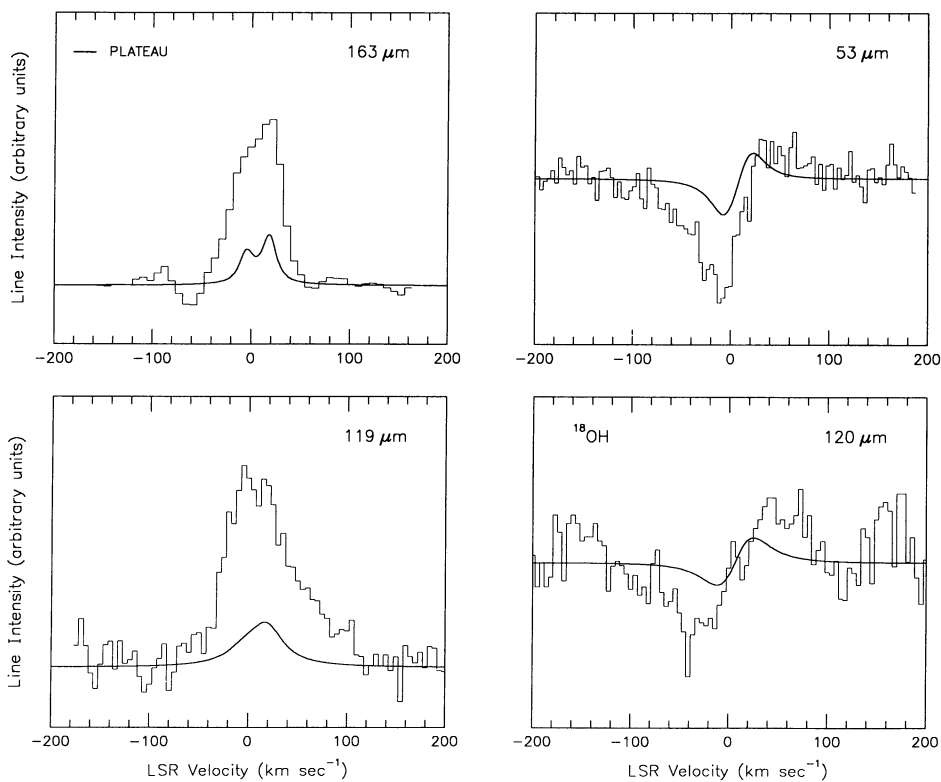


FIG. 9.—Same as Fig. 6, except for the contribution from the plateau alone. The intensity scale is the same as that used in Fig. 6, thus permitting a direct assessment of the relative contribution from the plateau to the final line profile.

resulting line profiles are at greater variance with the observations than emission from several components. In particular, for expected continuum backgrounds, emission from the shocked gas component alone results both in a slight P-Cygni profile for the ^{16}OH 119.234 μm line and a narrower ^{16}OH 163.121 μm line than is observed. The presence of a higher density region within the postshocked gas is suggested mostly by its effect on the line profiles; such a component, sharing in the 38 km s^{-1} velocity of the shock, serves to broaden all of the OH lines we observe. Supporting evidence for higher densities in the postshocked region, beyond the OH data presented here, is discussed in the next section.

Similarly, inclusion of the high-velocity plateau gas also serves to improve the fit between model and data. As is discussed below, corollary observational data from other species suggest that the plateau gas should be a source of OH emission. Finally, the mass of gas we assume for this component, $\sim 6 M_{\odot}$, is consistent with the mass estimate of high-velocity (i.e., $> 18 \text{ km s}^{-1}$) gas of $7 M_{\odot}$ derived from CO measurements (see Masson *et al.* 1984).

It is interesting to note that the ^{18}OH 120 μm and, to a lesser extent, the ^{16}OH 53 μm P-Cygni profiles indicate that there is no significant OH rotational emission from regions having both a v_{LSR} near $+9 \text{ km s}^{-1}$ and small internal gas velocities ($< 10 \text{ km s}^{-1}$). OH line emission from such regions at levels greater than $\sim 10\%$ of the total measured 120 and 53 μm line fluxes would begin to distort these line profiles in ways which are not seen. Thus, it is inferred that the hot core, compact ridge, and extended ridge are not major sources of OH rotational line radiation.

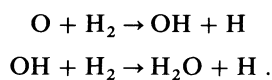
V. DISCUSSION

In this section we shall discuss the plausibility of our three-component model for the OH emission. Specifically, we review the reasons why the shocked gas region, the high-density postshock gas, and the plateau are reasonable OH sources, while the hot core and compact ridge may be less likely candidates for the OH emission we detect.

a) Postshocked Gas

The relatively fast moving ($v_s \sim 40 \text{ km s}^{-1}$) shock surrounding IRC2/BNKL provides a natural explanation for both the broad profiles observed in the 119 and 163 μm lines and the P-Cygni profiles seen in the 53 μm and ^{18}OH 120 μm transitions. Beyond this phenomenological association with the shocked gas region, the predicted abundance of OH within the postshock zone is sufficiently high that, under the prevailing density and temperature conditions, strong OH emission is expected from this gas.

Behind a C-type shock such as we consider here, the gas temperatures drop from a peak of ~ 3000 to $\sim 50 \text{ K}$ over a distance of $\sim 2\text{--}3 \times 10^{15} \text{ cm}$. Under these conditions, the gas phase abundance of OH is governed by relatively few reactions, the two most important being:



These reactions are endothermic, possessing activation energies of a few hundred degrees, but proceed rapidly once the thermal energy of the gas is sufficiently warm. For the profiles of temperature and density given by Draine and Roberge (1982) the above reactions yield an abundance of OH within

the postshocked gas, $f(\text{OH}) \{ \equiv [\text{N}(\text{OH})/\text{N}(\text{H}_2)] \}$, of between 2×10^{-5} and 4×10^{-7} . For a reasonable value of the shock radius, 43", and radiative background, $T_c = 80 \text{ K}$, the range of gas densities, temperatures, velocity gradients, and OH abundances given by the Draine and Roberge model (1982) comes close to accounting for the OH emission we observe.

b) High-Density Postshocked Zone

A better fit to the line profiles is obtained by assuming that the shock model described by Draine and Roberge possesses higher density gas in the postshocked zone than is assumed in their model. Supportive evidence for higher densities in the postshock flow is provided by recent observations of vibration-rotation and pure rotation lines of H_2 as well as CO vibration-rotation band emission toward H_2 Peak 1.

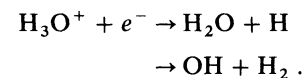
Recently, Brand *et al.* (1988) have reviewed the column densities needed to achieve the measured intensities of a total of 19 previously and newly detected H_2 lines from the shocked gas region in Orion-KL (H_2 Peak 1). Of particular interest here is their finding that the C-type shocks proposed by Draine and Roberge (1982) and Chernoff *et al.* (1982) may underestimate the column densities needed to explain the H_2 data at both high temperatures ($T_{\text{gas}} \geq 3 \times 10^3 \text{ K}$) and low temperatures ($T_{\text{gas}} \leq 1000 \text{ K}$) by about a factor of 10. At the higher temperatures this finding has little effect on the predicted OH line flux since the total column density of this hot gas is low. However, at the lower temperatures, the higher column densities are reflected in the line fluxes and profiles.

Similarly, the detection of the 4.7 μm fundamental vibration-rotation band of CO in emission toward H_2 Peak 1 (Geballe and Garden 1987) requires densities or column densities about an order of magnitude greater than those predicted by the C-type shock models. Specifically, a density of 10^7 cm^{-3} and a column density of $2 \times 10^{22} \text{ cm}^{-2}$ are necessary to excite the 4.7 μm fundamental vibration-rotation band into emission.

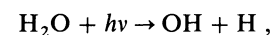
c) Plateau, Hot Core, and Compact Ridge

Like the shocked gas region, OH emission from the high-velocity gas in the plateau fits the observed line profiles. However, significant OH emission from the low-velocity gas within the hot core and compact ridge is not consistent with the measured ^{18}OH 120 μm P-Cygni profile. This distinction between regions likely results from a larger OH abundance in the plateau than either the hot core or compact ridge.

Within the warm gas found in the plateau, hot core, and compact ridge, OH can be formed in two ways. First, recombination of H_3O^+ can produce both H_2O and OH via the reaction



Second, even when H_2O is preferentially produced via the above reaction, the OH abundance subsequently can be increased by the photodissociation of water,



where the cross section for photodissociation is highest for photon wavelengths between 1000 and 1800 \AA . For the conditions within the plateau, hot core, and compact ridge, these processes lead to an $f(\text{OH})$ between 10^{-11} and 10^{-8} (S. Lepp, private communication), too low to result in significant far-infrared OH emission. However, recent observations of HDO

in Orion-KL by Plambeck and Wright (1987) and Walmsley *et al.* (1987) indicate an unexpectedly high HDO/H₂ abundance of $\sim 10^{-7}$ toward both the hot core and compact ridge which, like the anomalously high abundance of NH₃, HCN, CH₃OH, and NH₂D in these regions, is believed to be due to the evaporation of these species from dust grain mantles. H₂O released in this manner would be quickly converted to OH via photodissociation in those regions exposed to a strong ultraviolet (UV) field. That HDO is predominantly observed in the hot core and compact ridge, with only a small contribution from the plateau, suggests that shielding against UV photodissociation is less effective in the high-velocity gas. This would lead to a higher OH abundance in the plateau than either the hot core or compact ridge, which is consistent with our model. Significant OH emission from the extended ridge is not expected because of the low density ($\sim 10^5$ cm⁻³) and low temperature (~ 50 K) of this region.

VI. SUMMARY

We report the first detection of two important OH far-infrared, rotational transitions: (1) the ¹⁶OH ²Π_{1/2} → ²Π_{3/2} $J = 3/2^- \rightarrow 3/2^+$ cross-ladder transition at 53.351 μm and the ¹⁸OH ²Π_{3/2} $J = 5/2^+ \rightarrow 3/2^-$ rotational ground-state transition at 120.1719 μm. These data, along with previously obtained OH rotational line data, show the following:

1. The minimum ¹⁶OH column density toward Orion-KL is

4×10^{14} cm⁻² and the minimum OH abundance, $f(\text{OH})$, is 1.2×10^{-9} .

2. Radiative excitations play an important role in populating the rotational energy levels of OH in Orion-KL, as evidenced by the ratio of the ¹⁶OH 53.351 μm absorption and 163.396 μm emission intensities.

3. The width of the ¹⁶OH 119 and 163 μm lines along with the P-Cygni profiles exhibited by the ¹⁶OH 53 μm and ¹⁸OH 120 μm lines confirms that the origin of most of the OH emission we detect is associated with high-velocity gas in the outflow from the infrared cluster.

4. No single component model can account for the observed OH line fluxes and profiles.

5. The best fit to the data assumes that the OH emission arises within a C-type shock of the type described by Draine and Roberge (1982) and Chernoff *et al.* (1982) with a higher density postshocked region than given in these models. Emission from the plateau source also contributes to the OH flux we detect. All regions are subject to a strong infrared continuum background.

6. The hot core, compact ridge, and extended ridge do not contribute significantly to the detected OH emission.

We thank the staff of the Kuiper Airborne Observatory for their support. We also wish to acknowledge helpful discussions with M. Haggerty, S. Lepp, and C. Masson. This work was supported by NASA grants NAG 2-311 and NAG 2-208.

REFERENCES

- Beckwith, S., Persson, S. E., Neugebauer, G., and Becklin, E. E. 1978, *Ap. J.*, **223**, 464.
- Blake, G. A., Sutton, E. C., Masson, C. R., and Phillips, T. G. 1987, *Ap. J.*, **315**, 621.
- Brand, P. W. J. L., Moorhouse, A., Burton, M. G., Geballe, T. R., Bird, M., and Wade, R. 1988, *Ap. J. (Letters)*, **334**, L103.
- Chernoff, D. F., Hollenbach, D. J., and McKee, C. F. 1982, *Ap. J. (Letters)*, **259**, L97.
- Comben, E. R., Brown, J. M., Steimle, T. C., Leopold, K. R., and Evanson, K. M. 1986, *Ap. J.*, **305**, 513.
- Crawford, M. K., Lugten, J. B., Fitelson, W., Genzel, R., and Melnick, G. J. 1986, *Ap. J. (Letters)*, **303**, L57.
- Dewangan, D. P., Flower, D. R., and Alexander, M. H. 1987, *M.N.R.A.S.*, **226**, 505.
- Draine, B. T., and Roberge, W. G. 1982, *Ap. J. (Letters)*, **259**, L91.
- Erickson, E. F., Knacke, R. F., Tokunaga, A. T., and Haas, M. R. 1981, *Ap. J.*, **245**, 148.
- Geballe, T. R., and Garden, R. 1987, *Ap. J. (Letters)*, **317**, L107.
- Genzel, R., and Downes, D. 1982, in *Regions of Recent Star Formation*, ed. R. Roger and P. Dewdney (Dordrecht: Reidel), p. 251.
- Goldsmith, P. F., Krotkov, R., Snell, R. L., Brown, R. D., and Godfrey, P. 1983, *Ap. J.*, **274**, 184.
- Keene, J., Hildebrand, R. H., and Whitcomb, S. E. 1982, *Ap. J. (Letters)*, **252**, L11.
- Lugten, J. B. 1987, Ph.D. thesis, University of California, Berkeley.
- Masson, C. R., *et al.* 1984, *Ap. J. (Letters)*, **283**, L37.
- Melnick, G. J., Genzel, R., and Lugten, J. B. 1987, *Ap. J.*, **321**, 530 (Paper I).
- Plambeck, R. L., and Wright, M. C. H. 1987, *Ap. J. (Letters)*, **317**, L101.
- Schinke, R., and Andresen, P. 1984, *J. Chem. Phys.*, **81**, 5644.
- Sobolev, V. V. 1960, *Moving Envelopes of Stars* (Cambridge: Harvard University Press).
- Storey, J. W. V., Watson, D. M., and Townes, C. H. 1981, *Ap. J. (Letters)*, **244**, L27.
- van Dishoeck, E. F. 1984, Ph.D. thesis, University of Leiden.
- Viscuso, P. J., Stacey, G. J., Fuller, C. E., Kurtz, N. T., and Harwit, M. 1985a, *Ap. J.*, **296**, 142.
- Viscuso, P. J., Stacey, G. J., Harwit, M., Haas, M. R., Erickson, E. F., and Duffy, P. B. 1985b, *Ap. J.*, **296**, 149.
- Walmsley, C. M., Hermsen, W., Henkel, C., Mauersberger, R., and Wilson, T. L. 1987, *Astr. Ap.*, **172**, 311.
- Watson, D. M., Genzel, R., Townes, C. H., and Storey, J. W. V. 1985, *Ap. J.*, **298**, 316.
- Werner, M. W., Becklin, E. E., Gatley, I., and Neugebauer, G. 1977, in *Symposium on Recent Results in Infrared Astrophysics*, NASA Technical Memorandum (X-73, 190), p. 55.
- Werner, M. W., Crawford, M. K., Genzel, R., Hollenbach, D. J., Townes, C. H., and Watson, D. M. 1984, *Ap. J. (Letters)*, **282**, L81.
- Wynn-Williams, C. G., Genzel, R., Becklin, E. E., and Downes, D. 1984, *Ap. J.*, **281**, 172.

R. GENZEL and A. POGLITSCH: Max-Planck Institut für Physik und Astrophysik, Institut für Extraterrestrische Physik, D-8046 Garching, Federal Republic of Germany

J. B. LUGTEN: Institute for Astronomy, 2680 Woodlawn Drive, Honolulu, HI 96822

G. J. MELNICK: Center for Astrophysics, 60 Garden Street, Cambridge, MA 02138

G. J. STACEY: Department of Physics, Birge Hall, University of California, Berkeley, CA 94720